




# A novel and ultrasensitive non-enzymatic electrochemical glucose sensor in real human blood samples based on facile one-step electrochemical synthesis of nickel hydroxides nanoparticles onto a three-dimensional Inconel 625 foam

Rafiaa Kihal<sup>1,2</sup> · Hassina Fisl<sup>3</sup> · Mohamed Lyamine Chelaghmia<sup>1</sup>  · Widad Drissi<sup>1</sup> · Chahira Boukharouba<sup>1</sup> · Sara Abdi<sup>1</sup> · Mouna Nacef<sup>1</sup> · Abed Mohamed Affoune<sup>1</sup> · Maxime Pontié<sup>4</sup>

Received: 18 May 2022 / Accepted: 4 September 2022 / Published online: 17 September 2022  
© The Author(s), under exclusive licence to Springer Nature B.V. 2022

## Abstract

In this contribution, a simple and novel non-enzymatic electrochemical sensor for the detection of glucose was successfully prepared by direct in situ growth of nickel hydroxide nanoparticles ( $\text{Ni}(\text{OH})_2\text{NPs}$ ) onto a three-dimensional Inconel 625 foam (IN625F) substrate through a facile electrochemical route, using cyclic voltammetry (CV) method in alkaline medium without addition of nickel salts. Then, surface characterization of modified  $\text{Ni}(\text{OH})_2/\text{IN625F}$  electrodes was carried out through advanced technologies, such as scanning electron microscopy (SEM) and X-ray diffraction (XRD). The electrochemical catalytic behavior of the fabricated electrodes was investigated using CV and amperometric methods. The results revealed that the novel modified sensor,  $\text{Ni}(\text{OH})_2/\text{IN625F}$ , showed the highest sensitivity of  $5685 \mu\text{A}\text{mM}^{-1} \text{cm}^{-2}$  over a wide linear concentration range from 1 to 10 mM, with lowest detection limit (LOD) of  $2 \mu\text{M}$  ( $S/N=3$ ), and short response time within  $< 2$  s. Therefore, the proposed non-enzymatic electrochemical sensor demonstrated high selectivity and stability, good reproducibility, and low cost. In addition, analysis of human blood samples was performed. Hence, the constructed glucose sensor,  $\text{Ni}(\text{OH})_2/\text{IN625F}$ , with suitable performance could be used as a promising material in real human blood samples.

---

✉ Mohamed Lyamine Chelaghmia  
chelaghmia.mohamedlyamine@univ-guelma.dz;  
amine\_chelaghmia@yahoo.fr

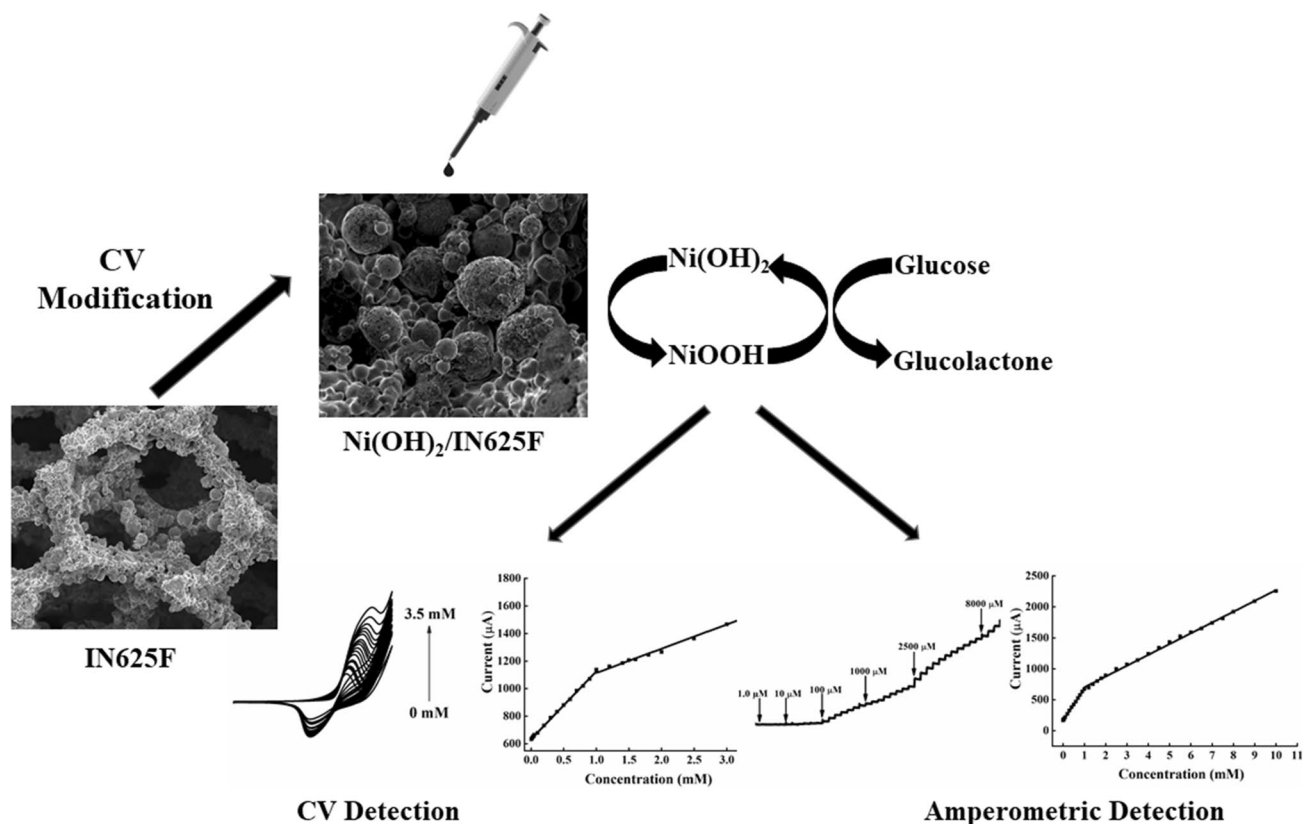
<sup>1</sup> Laboratoire d'Analyses Industrielles et Génie Des Matériaux, Université 8 Mai 1945 Guelma 24000, BP 401, Guelma, Algeria

<sup>2</sup> Université Abbes Laghrour Khenchela, BP 1252 Route de Batna, Khenchela 40004, Algeria

<sup>3</sup> Laboratoire de Chimie Appliquée, Université 8 Mai 1945 Guelma 24000, BP 401, Guelma, Algeria

<sup>4</sup> Univ. Angers, Group Analysis and Processes, 49045 Angers 01, France

## Graphical abstract



**Keywords** Inconel 625 foam · Nickel hydroxide · Non-enzymatic sensor · Glucose detection · EIS

## 1 Introduction

Carbohydrates are one of the most important sources of energy, providing a wide range of essential functions such as rapid digestibility, blood cholesterol control, and glucose regulation [1, 2]. Thus, diabetes mellitus is a common and serious chronic disease which is a significant public health problem, and often characterized by hyperglycemia. Therefore, determination of glucose concentration plays an important role in clinical diagnostics [3–7]. In fact, various methods have been frequently used for glucose detection, such as fluorescence spectroscopy [8], HPLC [9], electrochemiluminescence [10], and colorimetry [11]. However, these methods have some limitations in terms of time consumption and cost-effectiveness. To solve this problem, it's necessary to develop novel electrochemical glucose sensors with low cost, simplicity, stability, and portability [12–14].

Thereafter, electrochemical glucose sensors can be classified into two categories, based on their sensing mechanisms: enzyme-based biosensors and non-enzymatic

sensors. Then, enzyme-based biosensors are distinguished by their high cost of enzymes, instability, and poor reproducibility. Immobilization of glucose oxidase (GOx) is difficult on various substrates, and their performance is highly sensitive to changes in temperature, humidity, pH and substrate composition [15–17].

To address these issues, researchers have concentrated their efforts on developing and fabricating non-enzymatic glucose sensors with extended stability, fascinating sensitivity, simplicity, fast response, and outstanding catalytic performance [18–21]. Up to date, noble metals and their alloys, non-noble transition metals, and especially transition metal oxides/hydroxides have been considered as potential active materials for developing non-enzymatic glucose sensors, owing to their less expensive and more abundant on earth than noble metals [22, 23]. Diverse transition metal hydroxides, based on Ni(OH)<sub>2</sub> material, were proposed as a new kind of electrode configuration and shown improved electrochemical performance toward glucose molecules in an alkaline medium [24, 25]; the electrooxidation mechanism of glucose to glucolactone at electrode's surface might be significantly improved by the

well-known catalytic effect of the redox system Ni(OH)<sub>2</sub>/NiOOH [26–28].

Currently, significant advancements have been made in the fabrication of materials, such as metallic or intermetallic foams [29]. These new low-density materials have a unique combination of physical and chemical properties, allowing them to be used in a wide range of applications [30]. Among the different metallic foams, nickel foam (NF) is an ideal porous metal scaffold with a 3D network for growing Ni(OH)<sub>2</sub> NPs that has been used as a substrate for glucose sensors, owing to its low-density, high electronic conductivity, large surface area, and low cost [28].

Actually, various porous metal foams, such as Inconel 625 foam and 316L stainless steel foam, are widely used as conductive substrates for the deposition of Ni(OH)<sub>2</sub> NPs. Among them, Inconel 625 foam (IN625F) is a cubic nickel-based superalloy reinforced with a solid solution containing molybdenum and niobium on its nickel–chromium matrix [31, 32]. Compared to other foams, Inconel 625 foam exhibited better stability, in particular excellent resistance to corrosion and oxidation [33, 34]. However, to our knowledge, there are no reports have been found in the literature on the use of Inconel 625 foam as a new electrocatalyst material that can boost the electrocatalytic activity of non-enzymatic glucose sensing. Therefore, the modification of Inconel 625 foam with nickel hydroxide nanoparticles by direct in situ growth is beneficial to enlarge its active surface area, improve nano-confinement effect, as well as enhance its electrocatalytic performance.

In this work, we report for the first time the modification of an inactive and a novel commercially three-dimensional Inconel 625 foam electrode into an active and ultrasensitive non-enzymatic electrochemical glucose sensor, through the direct in situ growth of nickel hydroxide nanoparticles, using a facile and simple one-step electrochemical method in alkaline medium without nickel salts added. Further, scanning electron microscopy (SEM) and X-ray diffraction (XRD) techniques were used to characterize the surface of prepared Ni(OH)<sub>2</sub>/IN625F electrodes. Cyclic voltammetry (CV), electrochemical impedance spectroscopy (EIS), and amperometric measurements were used to investigate the electrochemical surface properties and electroanalytical performance of the fabricated sensors. In addition, analysis of real human blood samples by this non-enzymatic sensor was also performed with excellent stability and good reproducibility.

## 2 Experimental sections

### 2.1 Materials and reagents

All chemical reagents used in this work were of analytical grade. Sodium hydroxide (NaOH), potassium ferricyanide (K<sub>3</sub>Fe(CN)<sub>6</sub>), D-(+)-glucose (Glc), L(+)-ascorbic acid (AA), uric acid (UA), sucrose (Suc), and acetaminophen (AP) were purchased from Sigma–Aldrich and Fluka and were used without any purification. Commercial Inconel 625 foam was bought from Atlantum Company (Munich, Germany) and its chemical composition is depicted in Table 1. Samples of blood serum were acquired from a local hospital. Electrolytes were prepared with deionized water (DI).

### 2.2 Instruments

Electrochemical experiments were carried out using a potentiostat (Princeton Applied Research, AMETEK, USA) at room temperature. A 3-electrode setup was used, containing unmodified IN625 foam or modified Ni(OH)<sub>2</sub>/IN625F as the working electrodes, saturated calomel electrode (SCE) as the reference electrode, and platinum (Pt) wire as the counter electrode. All potentials values were cited versus SCE. CV, amperometric, and EIS measurements were used to assess the electrochemical surface properties and the electrocatalytic performance of modified Ni(OH)<sub>2</sub>/IN625F electrodes. CV measurements were carried out in the potential range of 0.0–0.7 V, with a fixed scan rate 50 mVs<sup>-1</sup>. Amperometric measurements were done at varied sensing potentials into a stirred alkaline medium. EIS technique was used in the frequency range of 100 to 0.1 Hz, with an amplitude voltage of 10 mV and a working potential of +0.5 V.

For glucose detection in real human blood samples by our prepared sensors, the current response of 25 µl real blood sample in 10 ml of NaOH 0.1 M solution was measured with an applied potential of +0.6 V. Surface morphology and crystalline structure of the as-prepared electrodes were examined by scanning electron microscopy (SEM) analysis using a JEOL JSM-IT 100, and X-ray diffraction (XRD) using a D8 Advance Bruker diffractometer (CuKα1, 2), respectively.

### 2.3 Preparation of modified Inconel 625 foam

Prior the modification, the open-cell Inconel 625 foam (IN625) substrates (0.5 × 0.2 cm) were ultrasonically soaked with acetone, ethanol, and then rinsed with deionized water. Next,

**Table 1** Chemical composition of Inconel 625 foam (wt.%)

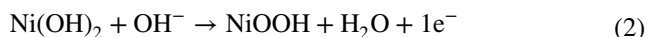
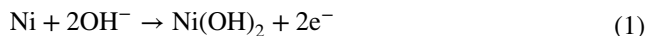
Element	Ni	Cr	Mo	Fe	Nb	Ti	Si	Al	S	Mn
Content	Bal	22.76	7.96	4.18	2.86	0.39	0.37	0.36	0.28	0.20

cleaned foams were dried in air at 100 °C for 2 h. Afterward, Inconel 625 foam substrates as working electrodes were activated to generate Ni(OH)<sub>2</sub> nanoparticles (NPs), using the 100 continuous CVs at 100 mV/s in alkaline solution (0.1 M NaOH) and in the range of 0.0 to 0.7 V. After reaching 100 cycles of CVs, the reproducible and stable CV curves were obtained. As a result, the modified Ni(OH)<sub>2</sub>/IN625F electrodes were designed and used as the active material for enzymeless glucose sensors.

### 3 Results and discussion

#### 3.1 Electrochemical formation and characterization of Ni(OH)<sub>2</sub>/IN625 foam

The active and stable nanoparticles of Ni(OH)<sub>2</sub> can be grown onto IN625 foam electrode via multiple scan cyclic voltammetry in 0.1 M NaOH solution. As observed in Fig. 1, a pair of well-defined redox peaks is obtained, in every voltammogram. So, the oxidation peak is due to the oxidation of Ni(OH)<sub>2</sub> phase to form NiO(OH), while the reduction peak is due to the reduction of NiO(OH) to form Ni(OH)<sub>2</sub>. Then, the proposed redox process may be represented by the following equations [26, 35–37]:



These peaks become more intense by increasing the number's cycles until reaching the 100<sup>th</sup> cycle, which indicated that the amount of Ni(OH)<sub>2</sub> deposited onto IN625 foam

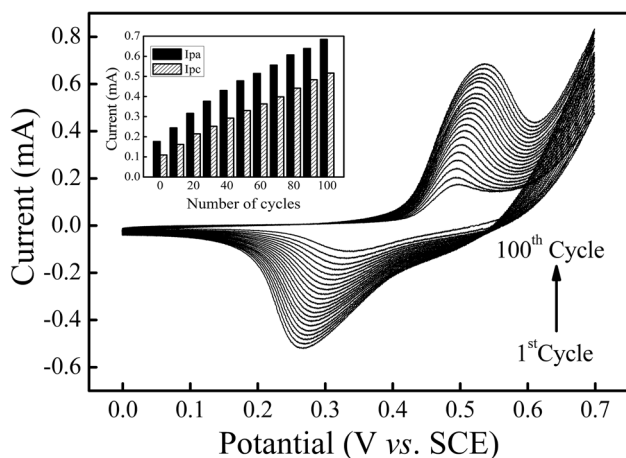


**Fig. 1** 100 cycles of CV curves recorded on Ni(OH)<sub>2</sub>/IN625F electrode preparation at 100 mV s<sup>-1</sup>, with inset [Illustration of anodic and cathodic peak currents against the number of cycles]

electrode surface was proportional to the plating time. After 100 cycles of CV scan, the anodic and cathodic peak currents values become stable (see Inset of Fig. 1), implying that the full surface of IN625 foam has been converted into Ni(OH)<sub>2</sub>.

These results indicate that Ni(OH)<sub>2</sub> NPs were successfully deposited onto IN625 foam via a simple electrochemical method. Furthermore, the main components of nickel-based IN625 foam, which are chromium and molybdenum, improve its structural stability and electrochemical reactivity. It is well known also that the redox Ni<sup>3+</sup>/Ni<sup>2+</sup> couple has excellent catalytic activity in alkaline medium. Then, Mo and Cr NPs aren't directly involved in the redox reaction like Ni atoms, but they are influenced by a synergetic combination with Ni to accelerate electron transport at the surface's electrode, improving the sensor's sensitivity to glucose detection.

SEM micrographs and XRD pattern of Ni(OH)<sub>2</sub>/IN625 foam electrodes are shown in Fig. 2. As illustrated in Fig. 2a, the foam has a three-dimensional cross-linked structure, containing spherical pores with an average size of 200 μm. It also has substantial and uniform wrinkles on its surface, which gives it high porosity, large specific surface area, and more active sites. As seen in SEM micrographs (b, c), Ni(OH)<sub>2</sub> nanoparticles were grown and well dispersed into IN625 foam surface after the activation process in an alkaline medium without the addition of nickel salts, forming a modified 3D super nanostructure foam adorned with Ni(OH)<sub>2</sub> NPs with an average particle size of about 40–50 nm. Figure 2d shows the X-ray diffraction pattern of the modified electrode. From this figure we observed, four peaks at angular positions of 19.33°, 51.88°, 60.18°, and 72.58° correspond to (001), (102), (003), and (201) diffractions of hexagonal β-Ni(OH)<sub>2</sub> structure (JCPDS cards No. 00–014–0117). The characteristic Ni(OH)<sub>2</sub> peaks are in good agreement with previous work reported by [23, 24, 28]. Furthermore, the crystalline peaks appeared at 44.53° and 72.58° were indexed to the diffraction planes of (411) and (2 12 1) of orthorhombic Ni–Cr–Mo alloy in IN625 foam (JCPDS cards No. 00–007–0050). In addition, the observed three peaks at 44.53°, 51.88°, and 76.40°, corresponding to (111), (200), and (220) crystalline planes of cubic phase Ni in IN625 foam (JCPDS cards No. 00–004–0850). Results of XRD confirmed the successful in situ growth of Ni(OH)<sub>2</sub> NPs onto IN625 foam.

#### 3.2 Electrochemical surface properties of Inconel 625 foam electrode

To evaluate the electrochemical properties of unmodified and modified IN625 foam electrodes through the ferricyanide system, CV and EIS were performed in 5 mM Fe(CN)<sub>6</sub><sup>3-</sup> as redox probe in an alkaline medium (0.05 M NaOH) at the



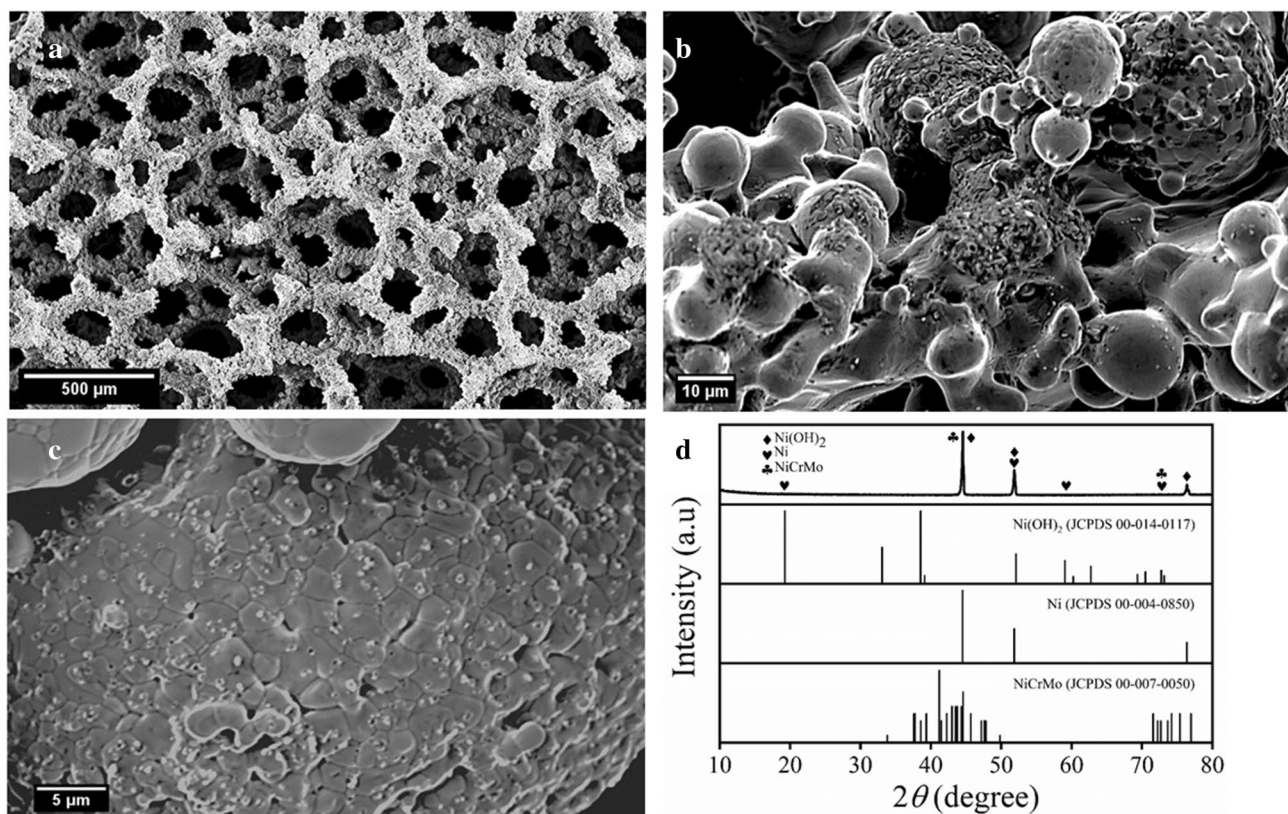


**Fig. 2** **a** Low, **b** medium and **c** high-magnification SEM images and **d** XRD pattern of Ni(OH)<sub>2</sub>/IN625 foam electrode

surface of both electrodes (Fig. 3). Figure 3a represents the overlay of the consecutive cyclic voltammograms of unmodified and modified foam electrodes, respectively, recorded at a potential sweep from 0.0 to 0.7 V and acquired at a scan rate of 50 mV s<sup>-1</sup>. From this figure, we observed in the first cycle of unmodified electrode two pairs of redox system which appear in all CVs and become more obvious as the number of cycles increases. The first pair located at 0.35 and 0.25 V, which assigned to the redox process of the ferrocyanide/ferricyanide couple, as follows [38]:



The second pair appeared at 0.65 and 0.45 V, due to the redox process of Ni<sup>2+</sup>/Ni<sup>3+</sup> according to the Eqs. (1–2) mentioned above. During the activation process, Ni-based IN625 foam surface electrode is oxidized into Ni(OH)<sub>2</sub>NPs, and its continued growth leads to a change in its electrochemical properties, which is explained in real time for the first time using Fe(CN)<sub>6</sub><sup>3-</sup> as redox probe. This is shown by the relationships between the anodic and cathodic peak currents and the peak-to-peak (ΔE<sub>p</sub>) separation with cycle's number, where both the anodic and cathodic peak currents of the ferrocyanide system, as well as the redox process of

Ni<sup>2+</sup>/Ni<sup>3+</sup>, gradually rise with increasing cycle's number (see Fig. 3b). Moreover, the peak-to-peak separation (ΔE<sub>p</sub>) of the ferrocyanide system was slightly decreased to 80 mV at the Ni(OH)<sub>2</sub>/IN625F compared to 120 mV for unmodified inconel foam (see Fig. 3c). These results indicate that the direct in situ growth of nickel hydroxide nanoparticles onto IN625 foam substrate improved the electrode surface area, providing more active sites for the glucose electrooxidation reaction, as well as increased conductivity, and the electron transfer rate at electrode/electrolyte solution interface.

The EIS was also used to study the interface properties of the unmodified and modified IN625 foam electrodes, under the same conditions as CV (see Fig. 3d). The Nyquist plot shows a semicircle part recorded at high frequencies, which correspond to a limited electron transfer process, and the diameter of the semi-circular part indicates the electron transfer resistance (R<sub>ct</sub>), in order to control the kinetics of electron transfer across the electrode/electrolyte interface. However, the modified Ni(OH)<sub>2</sub>/IN625F electrode with low diameter of the semi-circular portion shows a very low electron resistance and facilitated the interfacial conduction between electrode/electrolyte when compared with unmodified electrode. By fitting the impedance data with the equivalent circuit (see Fig. 3d, inset), the measured R<sub>ct</sub> value of Ni(OH)<sub>2</sub>/IN625F electrode (983.5 Ω) is nearly two times

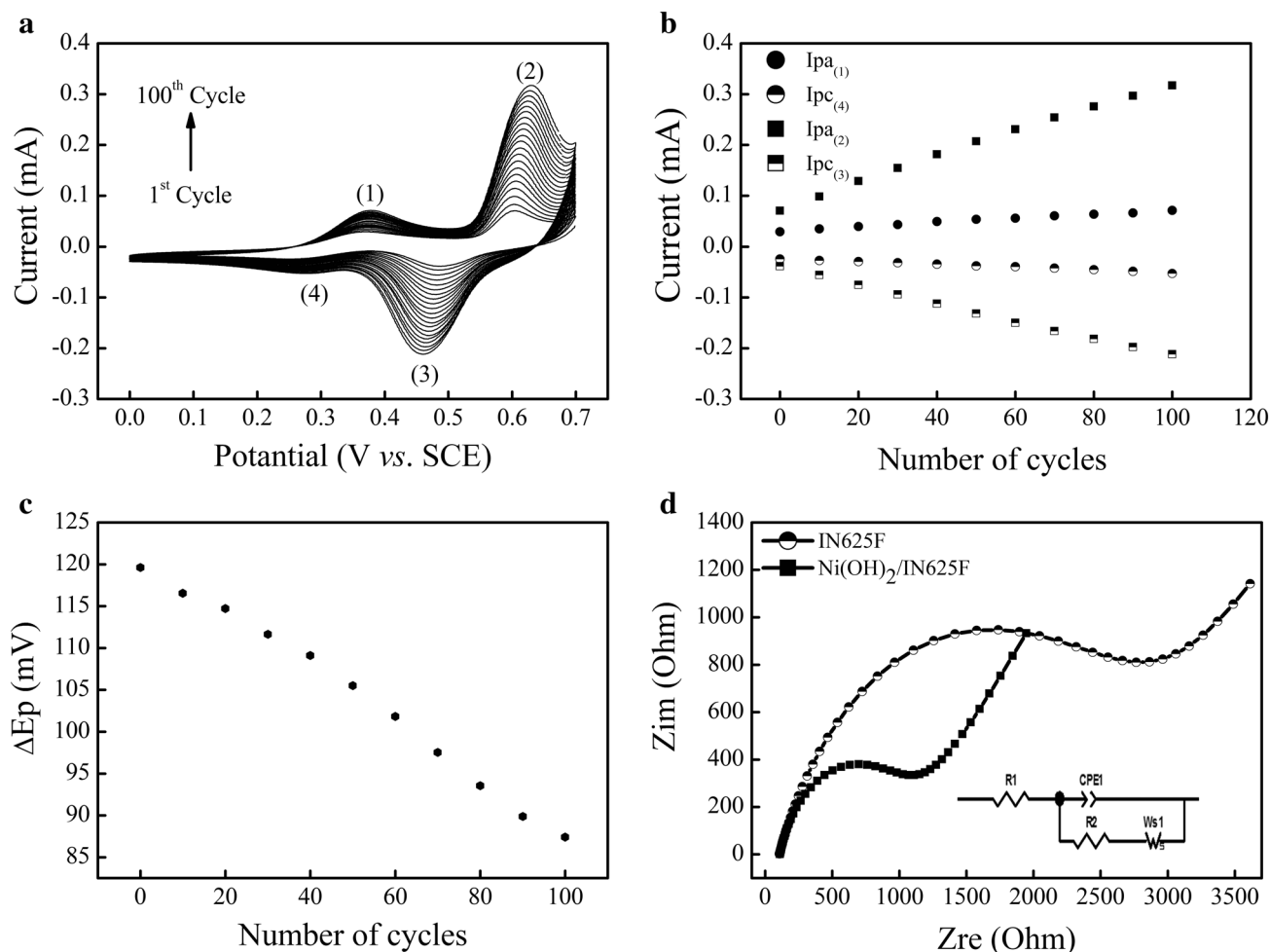


**Fig. 3** **a** CVs curves of 5 mM  $\text{Fe}(\text{CN})_6^{3-}$  in 0.05 M NaOH at  $\text{Ni}(\text{OH})_2/\text{IN625F}$  electrode, acquired at a fixed scan rate of  $50 \text{ mV s}^{-1}$  for 100 cycle, **b** Plots of anodic and cathodic peak currents vs. number

of cycles, **c** Peak-to-peak ( $\Delta E_p$ ) separation vs. number of cycles, **d** Nyquist plots obtained for unmodified and modified electrodes in 5 mM  $\text{Fe}(\text{CN})_6^{3-}$  solution prepared in 0.05 M NaOH [Inset: The equivalent circuit]

as low as that of the unmodified ( $2735 \Omega$ ) electrode. As a result, the activation has a significant effect on the electrochemical surface properties of the unmodified IN625 foam electrode by converting Ni into  $\text{Ni}(\text{OH})_2$ .

The electrochemical surface areas of unmodified IN625F and modified  $\text{Ni}(\text{OH})_2/\text{IN625F}$  electrodes were determined from the slopes of the curves  $I_p$  vs.  $v^{1/2}$  (see Fig. S1), using Randles–Sevcik’s equation, as follows [39]:

$$I_p = 0.436 nFAC \sqrt{\frac{nFDv}{RT}} \quad (4)$$

where  $I_p$  is the peak current (A),  $A$  is the electroactive area of the electrode ( $\text{cm}^2$ ),  $C$  is the bulk concentration ( $\text{mol cm}^{-3}$ ), and  $D$  is the diffusion coefficient ( $\text{cm}^2 \text{ s}^{-1}$ ), and  $v$  is the applied scan rate ( $\text{V s}^{-1}$ ). Through the calculation, the electroactive surface area of modified electrode is  $0.09$

$\text{cm}^2$ . This value is higher than  $0.06 \text{ cm}^2$  value of unmodified electrode. The results show that the proposed electrode’s surface area has been enlarged than unmodified electrode, due to the modification.

The effect of the potential scan rate on the electrochemical behavior of hydroxy and oxy-hydroxy-Ni species onto  $\text{Ni}(\text{OH})_2/\text{IN625F}$  electrode is also investigated by CV in 0.1 M NaOH solution, as presented in Fig. 4a. The anodic and cathodic peak currents are proportionate to the scan rate’s square root, and the well-defined redox peaks were clearly observed at various scan rates ranging from 10 to  $1000 \text{ mV s}^{-1}$ . Figure 4b shows an excellent linear relationship between peaks currents and sweep rate’s square root, as following equations:

$I_{pa} \text{ (mA)} = 0.613v^{1/2} [(\text{mVs}^{-1})^{1/2}] - 1.346$  and  $I_{pc} \text{ (mA)} = -0.591v^{1/2} [(\text{mVs}^{-1})^{1/2}] + 1.744$ , with high correlation coefficients of 0.999. This linearity suggests a

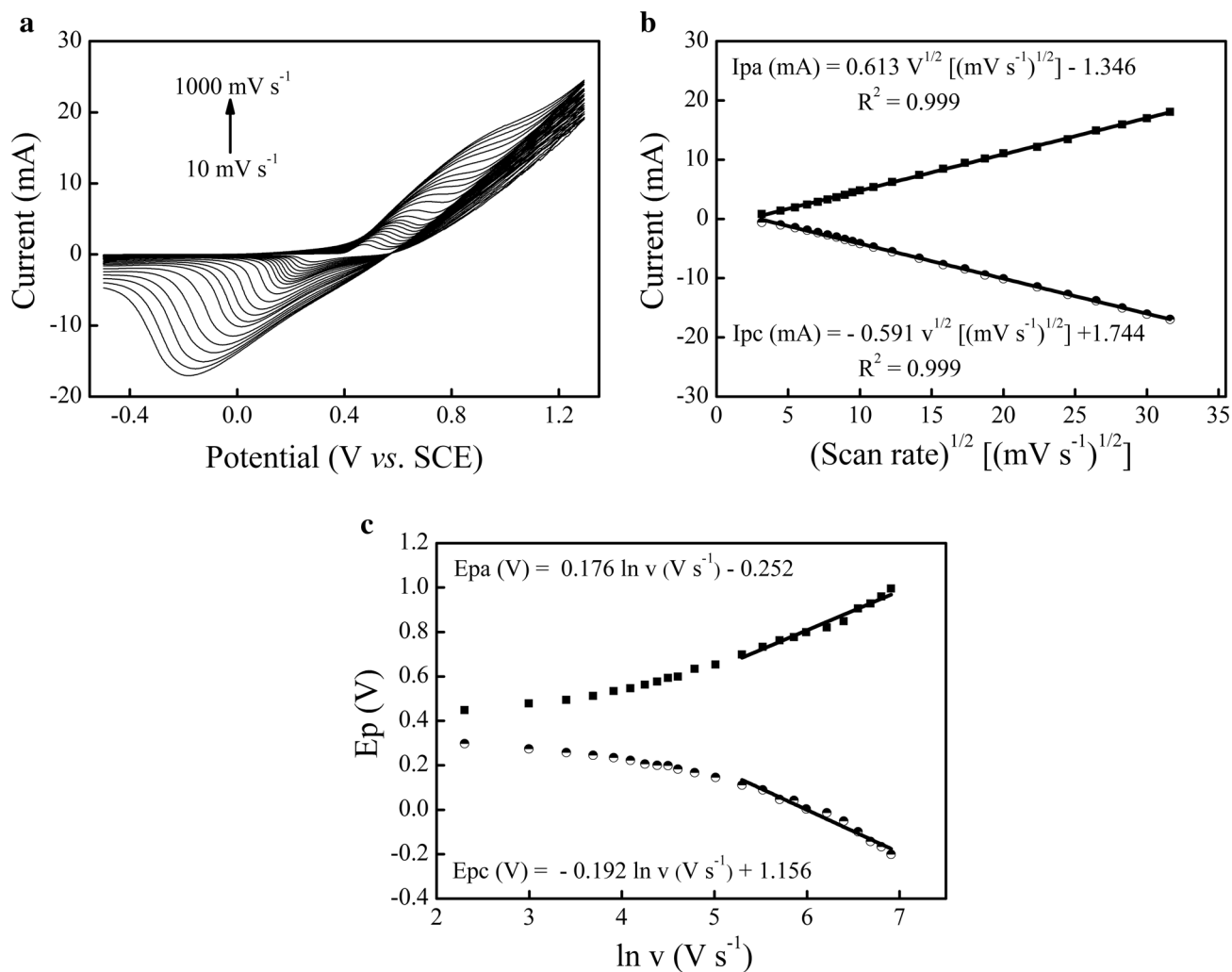


**Fig. 4** **a** CVs curves of Ni(OH)<sub>2</sub>/IN625F electrode in alkaline medium at scan rates of 10, 30, 50, 70, 100, 150, 200, 300, 400, 600, 800, and 1000 mV s<sup>-1</sup>, **b** Correlation plots between peak currents against scan rate's square root, **c** Plots of peaks potential versus lnv

diffusion-controlled process for the electrochemical reaction occurs over the Ni(OH)<sub>2</sub>/IN625F electrode surface.

The electrode surface coverage ( $\Gamma^*$ ) of the redox species of Ni(OH)<sub>2</sub> onto IN625F electrode can be determined using the following equation [40, 41]:

$$I_p = \left( \frac{n^2 F^2}{4RT} \right) v A \Gamma^* \tag{5}$$

where  $\Gamma^*$  is the surface coverage of redox species (mol cm<sup>-2</sup>). Then, the estimated  $\Gamma^*$  value was  $2.56 \times 10^{-8}$  mol cm<sup>-2</sup>. On the other hand, the electrochemical parameters related to modified electrodes such as the electron transfer coefficient ( $\alpha_s$ ) and electron transfer rate constant ( $K_s$ ) can be calculated from the CV response, owing to the surface-confined electroactive species of modified electrode at low concentration using Laviron's theory [42, 43]. For peak-to-peak potential

separation  $\Delta E_p > 200/n$  mV,  $E_{pa}$  and  $E_{pc}$  were expressed according to the following equations:

$$E_{pa} = E^o + [RT/(1 - \alpha)nF] \ln v \tag{6}$$

$$E_{pc} = E^o - (RT/\alpha nF) \ln v \tag{7}$$

$$\ln K_s = \alpha \ln(1 - \alpha) + (1 - \alpha) \ln \alpha - \ln(RT/nFv) - \alpha(1 - \alpha)nF\Delta E_p/RT \tag{8}$$

where  $E^o$  is the standard electrode potential (V) and the other terms have their usual meanings. At higher scan rates [400–1000 mV s<sup>-1</sup>], the peak potential demonstrates a linear relationship with the logarithmic function of scan rate, as seen in Fig. 4c. The estimated values of  $\alpha_s$  and  $K_s$  were found

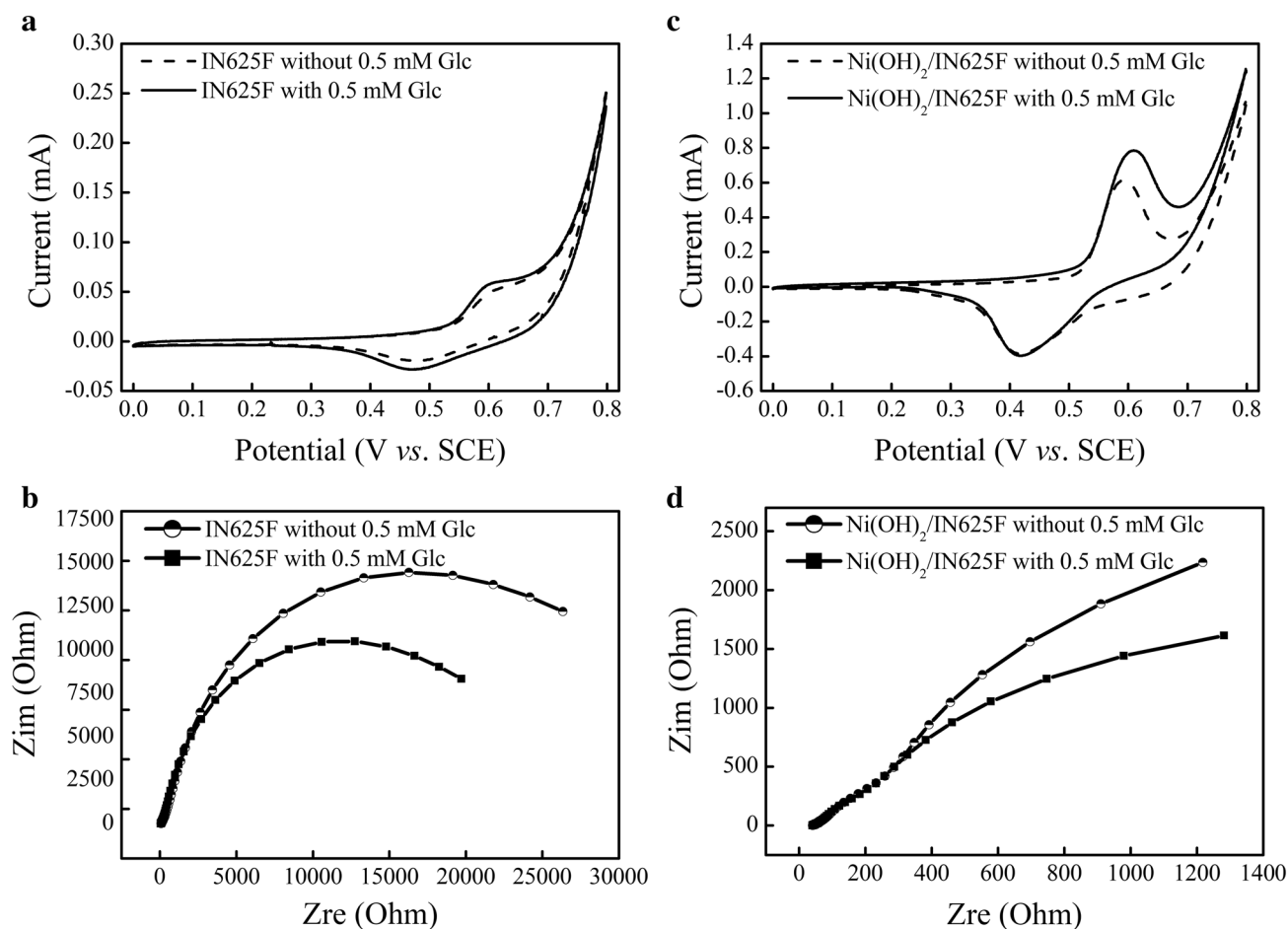


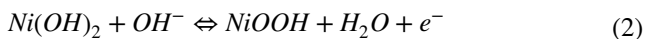
**Fig. 5** CVs responses of **a** IN625F, **b** Ni(OH)<sub>2</sub>/IN625F electrodes without and with 0.5 mM glucose addition in 0.1 M NaOH at a sweep rate 50 mVs<sup>-1</sup>. EIS responses of **c** IN625F, **d** Ni(OH)<sub>2</sub>/IN625F elec-

trodes without and with 0.5 mM glucose addition in 0.1 M NaOH at +0.5 V in the frequency range of 100 kHz at 0.1 kHz

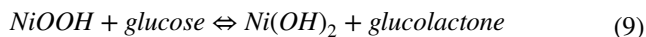
to be 0.37 and 1.18 s<sup>-1</sup>, respectively, using linear regression and Eqs. (6–8).

### 3.3 Electrocatalytic oxidation of glucose on IN625F and Ni(OH)<sub>2</sub>/IN625F electrodes

After the modification mentioned above, a comparative study on the electrocatalytic activity of unmodified IN625F and modified Ni(OH)<sub>2</sub>/IN625F electrodes to glucose oxidation was examined using CV and EIS techniques in the absence and presence of glucose. As shown in Fig. 5a, b, the CV curves of both electrodes without glucose addition revealed a pair of redox peaks, assigning to the redox couple of Ni<sup>+2</sup>/Ni<sup>+3</sup>, as follows [1, 37, 44]:



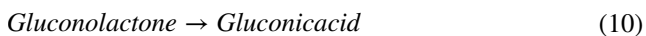
After the addition of glucose, the oxidation peak current at modified electrode is significantly larger than that at unmodified electrode, due to the excellent electrocatalytic property of Ni(OH)<sub>2</sub> NPs, and larger active surface area of the modified electrode. The mechanism for oxidation of glucose by Ni(OH)<sub>2</sub>-based material could be described by the following reaction [37, 44]:



In this reaction at anodic potentials, when glucose gradually diffuses to the electrode's surface, it's quickly oxidized to gluconolactone by strongly oxidizing Ni(III) species, which was simultaneously reduced to Ni(II). Therefore, the concentration of Ni(III) decreases while that of Ni(II) increases, resulting in an increase in anodic peak current and a decrease in cathodic peak current. The anodic peak potential shifted to a more positive potential, owing to the diffusion-limited process of glucose at the electrode's



surface. Finally, gluconolactone turned into gluconic acid by hydrolysis, as follows.



The results show the strong effect of the activation on the electrocatalytic oxidation of glucose at modified electrode surface compared with unmodified electrode.

Figure 5c, d compares the Nyquist plots of unmodified and modified electrodes in the absence and presence of glucose. The Nyquist plot of unmodified IN625F electrode in the absence of glucose showed a remarkable charge transfer resistance ( $R_{ct}$ ) about 22 k Ohm. However, when 0.5 mM of glucose was added, the  $R_{ct}$  value is decreased to 17 k Ohm than without glucose (see Fig. 5c). The estimated  $R_{ct}$  value of modified  $\text{Ni}(\text{OH})_2/\text{IN625F}$  electrode in the absence of glucose was around 6.2 k Ohm (see Fig. 5d). This value decreased more quickly by two times to reach 3.5 K Ohm than in the presence of glucose. The results revealed that the modified electrode exhibited a higher electrical conductivity and a much faster charge transfer phenomenon toward glucose oxidation than unmodified IN625F electrode. The result is well confirmed by CV.

In order to study the electrochemical kinetics of modified  $\text{Ni}(\text{OH})_2/\text{IN625F}$  electrode during the electrooxidation of glucose, CV curves were carried out in 0.1 M NaOH within 0.5 mM glucose at various scan rates, as marked in Fig. S2. With increasing scan rates, the anodic and cathodic peak's currents also increase (Supporting Information, Fig. S2a). Furthermore, the oxidation and reduction potentials, respectively, shifted to more positive and negative potentials. In addition, an excellent linear relationship between peaks currents and scan rate's square root with high correlation coefficient of 0.999 was exhibited in Fig. S2b, suggesting that the diffusion-controlled process governs the electrocatalytic oxidation of glucose on the surface of the modified  $\text{Ni}(\text{OH})_2/\text{IN625F}$  electrode, which is beneficial for voltametric and amperometric glucose sensing. Furthermore, the plot of  $\log I_p$  vs.  $\log \nu$  reveals excellent linearity, with a slope that is extremely close to the theoretical value of 0.5 (Fig. S2c), demonstrating that the modified  $\text{Ni}(\text{OH})_2/\text{IN625F}$  electrode showed a diffusion-controlled process for glucose oxidation.

### 3.4 Electroanalytical performance of $\text{Ni}(\text{OH})_2/\text{IN625F}$ electrode towards glucose detection

In order to demonstrate the glucose sensing application of  $\text{Ni}(\text{OH})_2/\text{IN625F}$  electrode, CV and amperometry techniques were both employed. Figure 6a illustrates CV curves of the proposed  $\text{Ni}(\text{OH})_2/\text{IN625F}$  electrode versus the sequential injections of glucose concentrations, at a constant scan rate of  $50 \text{ mVs}^{-1}$ . When glucose concentrations increased, the anodic peak currents gradually increased, while the cathodic peak currents decreased. Inset of Fig. 6a also shows the

anodic peak currents increased with lower glucose concentrations from  $4 \mu\text{M}$  to 0.05 mM. However, as presented in Fig. 6b, two linear responses are expressed as follows: one from  $4 \mu\text{M}$  to 1 mM represented by:  $I_p (\mu\text{A}) = 492.343C_{\text{GI}} (\text{mM}) + 634.073$  with  $R^2 = 0.999$  and the other from 1 mM to 3.5 mM displayed as follows:  $I_p (\mu\text{A}) = 175.615C_{\text{GI}} (\text{mM}) + 939.430$  with  $R^2 = 0.987$ . In addition, the sensitivity and detection limit (LOD) of the developed sensor were calculated to be  $5470 \mu\text{AmM}^{-1} \text{ cm}^{-2}$  and  $10 \mu\text{M}$ , respectively.

Figure 6c shows the amperometric curves of modified electrodes,  $\text{Ni}(\text{OH})_2/\text{IN625F}$ , carried out at three sensing potentials 0.5, 0.55, and 0.6 V, in order to find the optimum sensing potential by subsequent glucose injections. We noticed that all amperometric curves exhibited a considerable improvement in current responses occurred rapidly with successive injections of glucose within 2 s, indicating a rapid oxidation between glucose molecules and electrode's redox sites. The result showed that the proposed non-enzymatic  $\text{Ni}(\text{OH})_2/\text{IN625F}$  sensors had an outstanding sensitive and fast response toward glucose oxidation, under alkaline medium.

Figure 6d reveals three corresponding calibration plots resulting from the amperometric curves, demonstrating that all response currents increased linearly with subsequent glucose injections. As a result, linear slopes can be seen in the calibration graphs at various sensing potentials, due to the formation of intermediates, which are then adsorbed on the electrode's active sites, and reducing the number of  $\text{OH}^-$  catalytic sites, thus inhibiting the oxidation reaction of glucose. So, at sensing potential 0.5 V, the first calibration graph of the proposed sensor shows two linear ranges: one from  $1 \mu\text{M}$  to 1 mM represented by:  $I_p (\mu\text{A}) = 389.866C_{\text{GI}} (\text{mM}) + 15.617$  with  $R^2 = 0.998$  and the other from 1 to 8 mM expressed as follows:  $I_p (\mu\text{A}) = 128.110C_{\text{GI}} (\text{mM}) + 285.752$  with  $R^2 = 0.999$ . The second calibration graph at 0.55 V presents the first linear range from  $1 \mu\text{M}$  to 1 mM as the following equation:  $I_p (\mu\text{A}) = 438.042C_{\text{GI}} (\text{mM}) + 47.664$  with  $R^2 = 0.999$  and the second linear range from 1 to 8 mM is as follows:  $I_p (\mu\text{A}) = 166.401C_{\text{GI}} (\text{mM}) + 318.391$  with  $R^2 = 0.998$ . Finally, the third calibration plot at 0.6 V illustrates the following: one from  $1 \mu\text{M}$  to 1 mM expressed by:  $I_p (\mu\text{A}) = 511.668C_{\text{GI}} (\text{mM}) + 167.666$  with  $R^2 = 0.999$ , and the other from 1 to 10 mM displayed as follows:  $I_p (\mu\text{A}) = 174.469C_{\text{GI}} (\text{mM}) + 529.541$  with  $R^2 = 0.998$ . The calculated sensitivity of the prepared sensors at sensing potential of 0.5, 0.55, and 0.6 V was found to be 4332, 4867 and  $5685 \mu\text{A mM}^{-1} \text{ cm}^{-2}$ , respectively. Then, the limit of detection (LOD) was estimated to be 11, 4 and  $2 \mu\text{M}$  ( $S/N=3$ ) for  $\text{Ni}(\text{OH})_2/\text{IN625F}$  sensors at sensing potentials 0.5, 0.55 and 0.6 V, respectively.

As a result, the electrocatalytic performance of  $\text{Ni}(\text{OH})_2/\text{IN625F}$  sensor with optimum sensing potential 0.6 V

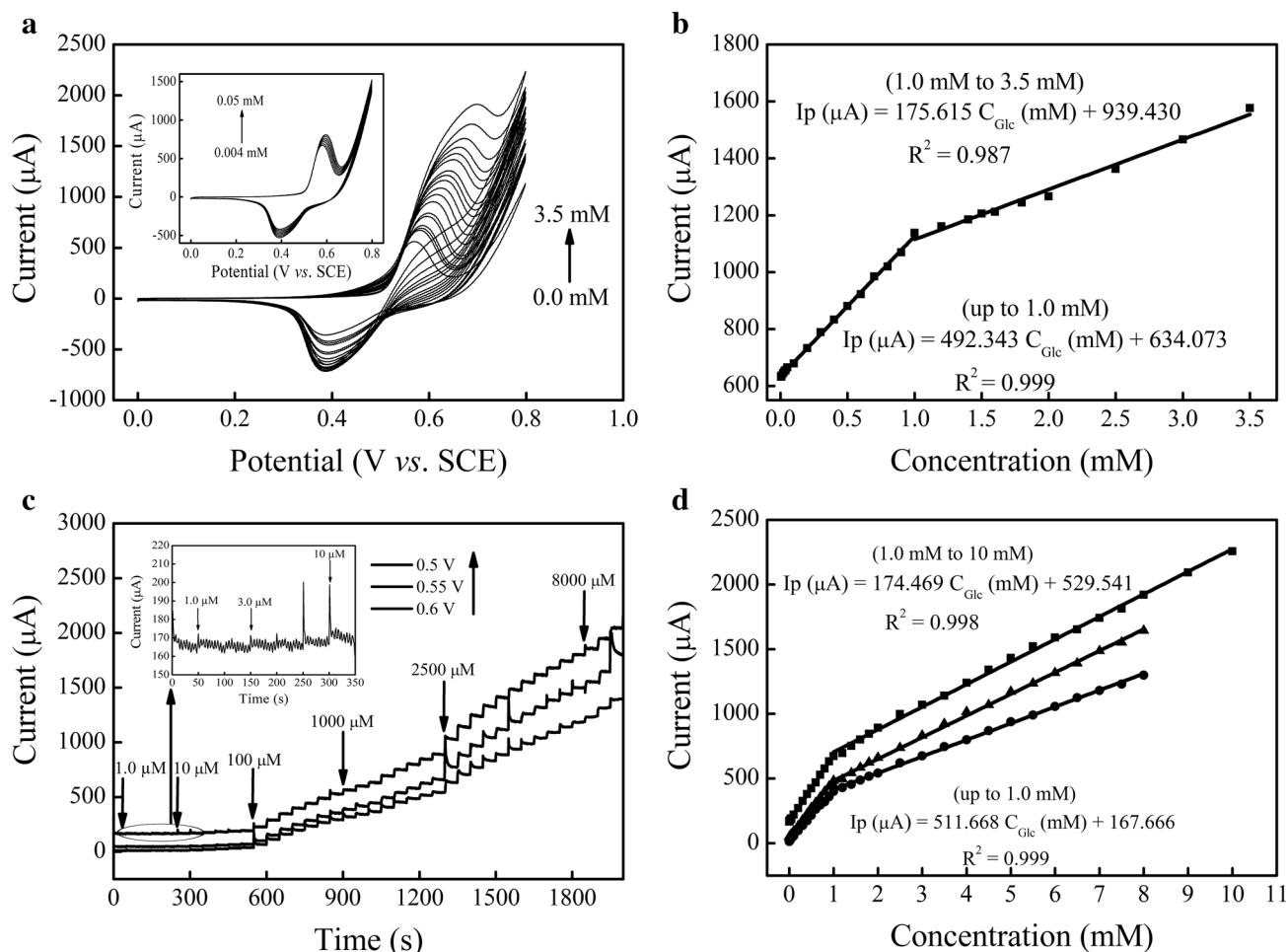


**Fig. 6** **a** Ni(OH)<sub>2</sub>/IN625F sensor CVs with consecutive injections of glucose concentrations at 50 mVs<sup>-1</sup> with inset: [CVs with lower glucose concentrations], **b** Plot of *I*<sub>pa</sub> vs. concentration, **c** Typical amperometric responses of Ni(OH)<sub>2</sub>/IN625F sensors, carried out at varied

sensing potentials into a stirred 0.1 M NaOH within subsequent glucose injections, with inset: [i-t curve toward the addition of glucose 1–10 μM], **d** Corresponding calibration curves of *I*<sub>pa</sub> vs. concentra-

tion showed the highest sensitivity, widest linear range, and lowest limit of detection when compared with other sensors at 0.5 and 0.55 V sensing potentials, suggesting that the newly proposed electrode appears to be a promising contender for non-enzymatic electrochemical glucose sensing. Table 2 also compares the obtained analytical performance of our newly proposed glucose sensor to others based on Ni foams previously reported in the literature.

### 3.5 Anti-interference, reproducibility, and stability of Ni(OH)<sub>2</sub>/IN625F sensor

The effect of some common interfering species present in human blood serum, such as L-ascorbic acid, acetaminophen, uric acid, and sucrose, on the electrochemical response of Ni(OH)<sub>2</sub>/IN625F sensor toward glucose, was examined using an amperometry technique into a stirred 0.1 M NaOH solution with subsequent 1 mM glucose

injections and 0.1 mM of interferences at sensing potential 0.6 V. As shown in Fig. 7a, there are insignificant current responses toward interferences (less than 4%) on the amperometric curves when compared to glucose, implying that the fabricated Ni(OH)<sub>2</sub>/IN625F as non-enzymatic sensor has an excellent selectivity toward glucose in the vicinity of interfering species. In addition, the current response of 1.0 mM glucose was measured to assess the reproducibility of five Ni(OH)<sub>2</sub>/IN625F sensors that were independently prepared under the same conditions, as shown in Fig. S3. The estimated relative standard deviation (RSD) was found to be 4.98%, indicating that the various designed sensors had a good reproducibility. Therefore, to evaluate the repeatability, five consecutive CV measurements of 1.0 mM glucose were taken using the same sensor (see Fig. S4). The estimated RSD of the response current was 2.39%, suggesting that the Ni(OH)<sub>2</sub>/IN625F sensor has excellent repeatability and is not contaminated by glucose oxidation products. Therefore,

**Table 2** Comparison of the performance of newly designed Ni(OH)<sub>2</sub>/IN625F sensor with other glucose sensors based on Ni foam

Electrode	Sensitivity ( $\mu\text{A mM}^{-1} \text{cm}^{-2}$ )	Linear range (mM)	LOD ( $\mu\text{M}$ )	References
$\alpha$ -Ni(OH) <sub>2</sub> -rGO/NiF <sup>a</sup>	95.5	0.5–22.5	–	[45]
NiO superstructures/NiF <sup>b</sup>	395	0.018–1.2	6.15	[46]
Ni(OH) <sub>2</sub> /NiF <sup>c</sup>	1130	0.002–0.04	1	[47]
Ni(OH) <sub>2</sub> nanowires /NiF <sup>d</sup>	1598	0.1–6	1	[48]
PDs–NiCo <sub>2</sub> O <sub>4</sub> /NiF <sup>e</sup>	806.17	0.005–0.25	2.75	[49]
Nifoam <sup>f</sup>	–	0.05–7.35	2.2	[50]
Ni <sub>3</sub> S <sub>2</sub> NS/NiF <sup>g</sup>	6148.0	0.005–3.0	1.2	[51]
ZnCo <sub>2</sub> O <sub>4</sub> /NiF <sup>h</sup>	15.64	0.1–3	4	[52]
Ni/NiF <sup>i</sup>	2370	0.01–0.7	5	[53]
CoPO MA/NiF <sup>j</sup>	3550	0.001–1.16	1	[54]
Ni(OH) <sub>2</sub> flakes/NiF <sup>k</sup>	2617.4	0.0025–1.05	2.5	[55]
NiCo <sub>2</sub> O <sub>4</sub> NWs/NiF <sup>l</sup>	5916	0.001–3.987	0.94	[56]
Ni–Al–Mn/NiF <sup>m</sup>	2253	0.015–2	1.49	[57]
Ni(OH) <sub>2</sub> / IN625F	5685	0.001–10	2	This work

<sup>a</sup> $\alpha$ -nickel hydroxide Ni(OH)<sub>2</sub>-reduced graphene oxide (rGO) nanocomposite on nickel foam

<sup>b</sup>nickel oxide (NiO) superstructures on nickel foam

<sup>c</sup>nickel hydroxide Ni(OH)<sub>2</sub> nanosheets on nickel foam

<sup>d</sup>nickel hydroxide Ni(OH)<sub>2</sub> nanowires on nickel foam

<sup>e</sup>Polymer dot (PD) bridged nickel cobalt oxide (NiCo<sub>2</sub>O<sub>4</sub>)-coated Ni foam

<sup>f</sup>nickel foam

<sup>g</sup>Nickel sulfide(Ni<sub>3</sub>S<sub>2</sub>) nanoflakes (NS) on nickel foam

<sup>h</sup>Zinc cobaltite (ZnCo<sub>2</sub>O<sub>4</sub>) on nickel foam

<sup>i</sup>nickel (Ni) nanoparticles on nickel foam

<sup>j</sup>cobalt phosphate (CoPO) microsheet arrays (MA) supported on Ni foam

<sup>k</sup>nickel hydroxide Ni(OH)<sub>2</sub> flakes on nickel foam

<sup>l</sup>nickel cobalt oxide (NiCo<sub>2</sub>O<sub>4</sub>) nanowires on nickel foam

<sup>m</sup>Hollow Ni–Al–Mn triple layered hydroxide (HLTH) nanocomposites-modified Ni foam

this sensor can be used repeatedly. Thereafter, the amperometric response curves were recorded every fifteen days over two months to examine the stability of Ni(OH)<sub>2</sub>/IN625F sensor, as shown in Fig. 7b. So, the sensor was kept dry between two measurements. The results showed only a reduction in the current response of 6.4% for 1.0 mM glucose in an alkaline medium (0.1 M NaOH) at 0.6 V, indicating that the Ni(OH)<sub>2</sub>/IN625F sensor has a higher stability when stored in the environment.

### 3.6 Glucose detection in blood serum samples

The Ni(OH)<sub>2</sub>/IN625F sensor's feasibility was further tested utilizing the same glucose concentrations in human blood serums, as well as a standard sample. The Ni(OH)<sub>2</sub>/IN625F sensor had a close current response, as illustrated in Fig. 7c, indicating that it might be used in real applications. Thereafter, the applicability of newly Ni(OH)<sub>2</sub>/IN625F sensor for real blood samples was examined by a commercial glucometer and then by our proposed sensor using amperometric measurements. I-t curves were recorded at 0.6 V (see

Fig. 7d) and the findings were gathered in Table 3. The proposed sensor gave us the recoveries varied from 93.27 to 103.60%. The results suggest that newly Ni(OH)<sub>2</sub>/IN625F sensor is recommended to glucose determination in real human blood.

## 4 Conclusions

For the first time, Ni(OH)<sub>2</sub> nanoparticles were successfully grown onto Inconel 625 foam via a simple and facile electrochemical route using CV method in an alkaline medium without addition of nickel salts. Electrochemical surface properties of Inconel 625 foam electrodes during the activation process were explained by CV method for the first time in real time using potassium ferricyanide as redox probe. Analytical performance of the prepared sensors was studied by cyclic voltammetry and amperometric measurements. As a result, the IN625 foam electrode was successfully modified, and its electrochemical properties were improved. The results show that the activation has a significant effect on

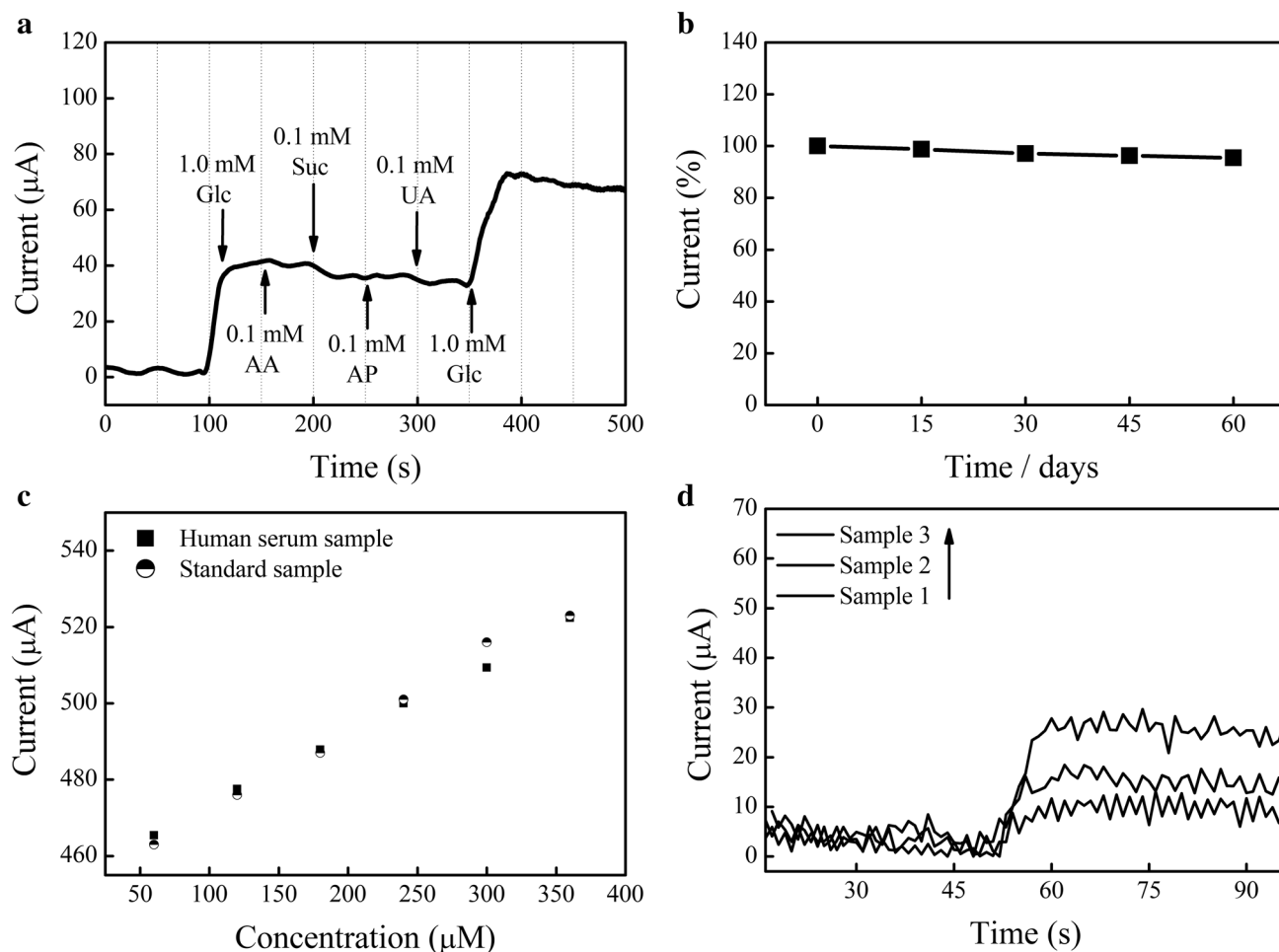


**Fig. 7** **a** Amperometric current–time of  $\text{Ni}(\text{OH})_2/\text{IN625F}$  sensor with stirred successive additions of 1 mM glucose and interfering species of 0.1 mM uric acid, 0.1 mM ascorbic acid, 0.1 mM sucrose and 0.1 mM acetaminophen, **b** Illustration of current–time of  $\text{Ni}(\text{OH})_2/\text{IN625F}$  sensor toward 1 mM glucose in 0.1 M NaOH for two months,

**c** Responses of  $\text{Ni}(\text{OH})_2/\text{IN625F}$  sensor to the same glucose concentrations in human blood sample and in a standard sample, **d** Amperometric current–time of  $\text{Ni}(\text{OH})_2/\text{IN625F}$  sensor in a stirred 0.1 M NaOH containing human blood serum at 0.6 V

**Table 3** Practicality of the newly amperometric sensor for detecting glucose in human blood serum samples

Samples	Concentration of glucose (mM)		Recovery (%)
	Proposed non-enzymatic method (mM)	Determined by a commercial glucometer (mM)	
1	3.72	3.47	93.27
2	7.77	8.05	103.60
3	24.03	24.28	101.04

the electrochemical surface properties of IN625 foam electrode by converting Ni into  $\text{Ni}(\text{OH})_2$ . The novel modified sensor,  $\text{Ni}(\text{OH})_2/\text{IN625F}$ , with optimum sensing potential of 0.6 V characterized by a large surface area, showed also the highest sensitivity of  $5685 \mu\text{A} \text{mM}^{-1} \text{cm}^{-2}$  over a wide

linear concentration range from 1  $\mu\text{M}$  to 10 mM, with faster response time  $< 2$  s, as well as lowest detection limit (LOD) of 2  $\mu\text{M}$ . Therefore, the fabricated sensor,  $\text{Ni}(\text{OH})_2/\text{IN625F}$ , exhibited a fascinating selectivity in the vicinity of interfering species, high stability, and good reproducibility. In addition, the results revealed also good recoveries to glucose in human blood serum samples. Thus, the newly designed glucose sensor,  $\text{Ni}(\text{OH})_2/\text{IN625F}$ , with suitable performance and low cost could be used as a promising device for real sample analysis.

**Acknowledgements** The financial support within the General Direction of Scientific Research and Technology Development of the Algerian Ministry of Higher Education and Scientific Research is greatly acknowledged.



## Declarations

**Conflict of interest** The authors declare no competing financial interest.

## References

- Li H, Zhang L, Mao Y, Wen C, Zhao P (2019) A simple electrochemical route to access amorphous Co-Ni hydroxide for nonenzymatic glucose sensing. *Nanoscale Res Lett* 14:135. <https://doi.org/10.1186/s11671-019-2966-2>
- Ojani R, Raoof JB, Fathi S (2012) Nickel/poly(o-aminophenol) film prepared in presence of sodium dodecyl sulfate: application for electrocatalytic oxidation of carbohydrates. *J Chin Chem Soc* 59:788–792. <https://doi.org/10.1002/jccs.201100463>
- Wang Q, Zhang Y, Ye W, Wang C (2016) Ni(OH)<sub>2</sub>/MoS<sub>x</sub> nanocomposite electrodeposited on a flexible CNT/PI membrane as an electrochemical glucose sensor: the synergistic effect of Ni(OH)<sub>2</sub> and MoS<sub>x</sub>. *J Solid State Electrochem* 20:133–142. <https://doi.org/10.1007/s10008-015-3002-9>
- King H, Aubert RE, Herman WH (1998) Global burden of diabetes, 1995–2025: prevalence, numerical estimates, and projections. *Diabetes Care* 21:1414–1431. <https://doi.org/10.2337/diacare.21.9.1414>
- Zhe T, Sun X, Liu Y, Wang Q, Li F, Bu T, Jia P, Lu Q, Wang J, Wang L (2019) An integrated anode based on porous Ni/Cu(OH)<sub>2</sub> nanospheres for nonenzymatic glucose sensing. *Microchem J* 151:104197. <https://doi.org/10.1016/j.microc.2019.104197>
- Rungsawang T, Punrat E, Adkins J, Henry C, Chailapakul O (2016) Development of electrochemical paper-based glucose sensor using cellulose-4-aminophenylboronic acid-modified screen-printed carbon electrode. *Electroanalysis* 28:462–468. <https://doi.org/10.1002/elan.201500406>
- Naik KK, Ratha S, Rout CS (2016) Phase and shape dependent non-enzymatic glucose sensing properties of nickel molybdate. *Chemistry Select* 1:5187–5195. <https://doi.org/10.1002/slct.201600795>
- Klonoff DC (2012) Overview of fluorescence glucose sensing: a technology with a bright future. *J Diabetes Sci Technol* 6:1242–1250. <https://doi.org/10.1177/193229681200600602>
- Filip M, Vlassa M, Coman V, Halmagyi A (2016) Simultaneous determination of glucose, fructose, sucrose and sorbitol in the leaf and fruit peel of different apple cultivars by the HPLC–RI optimized method. *Food Chem* 199:653–659. <https://doi.org/10.1016/j.foodchem.2015.12.060>
- Kremeskovter J, Wilson R (1995) Detection of glucose via electrochemiluminescence in a thin-layer cell with a planar optical waveguide. *Meas Sci Technol* 6:1325–1328. <https://doi.org/10.1088/0957-0233/6/9/012>
- Morikawa MA, Kimizuka N (2002) New colorimetric detection of glucose by means of electron-accepting indicators: ligand substitution of [Fe(acac)<sub>3-n</sub>(phen)<sub>n</sub>]<sup>3+</sup> complexes triggered by electron transfer from glucose oxidase. *Chem Eur J* 8:5580–5584. [https://doi.org/10.1002/1521-3765\(20021216\)8:24%3c5580:AID-CHEM5580%3e3.0.CO;2-V](https://doi.org/10.1002/1521-3765(20021216)8:24%3c5580:AID-CHEM5580%3e3.0.CO;2-V)
- Li HB, Zhao P (2019) Amorphous Ni-Co-Fe hydroxide nanospheres for the highly sensitive and selective non-enzymatic glucose sensor applications. *J Alloys Compd* 800:261–271. <https://doi.org/10.1016/j.jallcom.2019.05.264>
- Liu B, Li Z (2019) Electrochemical treating of a smooth Cu-Ni-Zn surface into layered micro-chips of rice grain-like Cu/Ni(OH)<sub>2</sub> nanocomposites as a highly sensitive enzyme-free glucose sensor. *J Electroanal Chem* 855:113493. <https://doi.org/10.1016/j.jelechem.2019.113493>
- Wang L, Nie F, Zheng J (2013) Nickel hydroxide and intercalated graphene with ionic liquid nanocomposite modified electrode for sensing of glucose. *J Chin Chem Soc* 60:1062–1069. <https://doi.org/10.1002/jccs.201200587>
- Chelaghmia ML, Nacef M, Affoune AM, Pontie M, Derabla T (2018) Facile synthesis of Ni(OH)<sub>2</sub> modified disposable pencil graphite electrode and its application for highly sensitive non-enzymatic glucose sensor. *Electroanalysis* 30:1117–1124. <https://doi.org/10.1002/elan.201800002>
- Wang L, Lu X, Ye Y, Sun L, Song Y (2013) Nickel-cobalt nanostructures coated reduced graphene oxide nanocomposite electrode for nonenzymatic glucose biosensing. *Electrochim Acta* 114:484–493. <https://doi.org/10.1016/j.electacta.2013.10.125>
- Sim H, Kim JH, Lee SK, Song MJ, Yoon DH, Lim DS, Hong SI (2012) High-sensitivity non-enzymatic glucose biosensor based on Cu(OH)<sub>2</sub> nanoflower electrode covered with boron-doped nanocrystalline diamond layer. *Thin Solid Films* 520:7219–7223. <https://doi.org/10.1016/j.tsf.2012.08.011>
- Nacef M, Chelaghmia ML, Affoune AM, Pontie M (2019) Electrochemical investigation of glucose on a highly sensitive nickel-copper modified pencil graphite electrode. *Electroanalysis* 31:113–120. <https://doi.org/10.1002/elan.201800622>
- Boukharouba C, Nacef M, Chelaghmia ML, Kihal R, Drissi W, Fislis H, Affoune AM, Pontie M (2022) Dendritic Cu(OH)<sub>2</sub> nanostructures decorated pencil graphite electrode as a highly sensitive and selective impedimetric non-enzymatic glucose sensor in real human serum blood samples. *Monatsh Chemie* 153:171–181. <https://doi.org/10.1007/s00706-021-02883-8>
- Rinaldi AL, Sobral S, Carballo R (2017) Nickel hydroxide nanoparticles on screen printed electrodes as an impedimetric non-enzymatic glucose sensor. *Electroanalysis* 29:1961–1967. <https://doi.org/10.1002/elan.201700187>
- Marini S, Ben Mansour N, Hjiri M, Dhahri R, Mir El, Espiro LC, Bonavita A, Galvagno S, Neri G, Leonardi SG (2018) Non-enzymatic glucose sensor based on nickel/carbon composite. *Electroanalysis* 30:727–733. <https://doi.org/10.1002/elan.201700687>
- Chelaghmia ML, Nacef M, Fislis H, Affoune AM, Pontie M, Makhlof A, Derabla T, Khelifi O, Aissat F (2020) Electrocatalytic performance of Pt-Ni nanoparticles supported on an activated graphite electrode for ethanol and 2-propanol oxidation. *RSC Adv* 10:36941–36948. <https://doi.org/10.1039/D0RA07331H>
- Wu X, Li F, Zhao C, Qian X (2018) One-step construction of hierarchical Ni(OH)<sub>2</sub>/RGO/Cu<sub>2</sub>O on Cu foil for ultra-sensitive non-enzymatic glucose and hydrogen peroxide detection. *Sens Actuators B Chem* 274:163–171. <https://doi.org/10.1016/j.snb.2018.07.141>
- Yang D, Gao L, Yang JH (2017) Facile synthesis of ultrathin Ni(OH)<sub>2</sub>-Cu<sub>2</sub>S hexagonal nanosheets hybrid for oxygen evolution reaction. *J Power Sources* 359:52–56. <https://doi.org/10.1016/j.jpowsour.2017.05.034>
- Liu P, Qin K, Wen S, Wang L, He F, Liu E, He C, Li CSJ, Li Q, Ma L, Zhao N (2018) In situ fabrication of Ni(OH)<sub>2</sub>/Cu<sub>2</sub>O nanosheets on nanoporous NiCu alloy for high performance supercapacitor. *Electrochim Acta* 283:970–978. <https://doi.org/10.1016/j.electacta.2018.07.007>
- Kung CW, Cheng YH, Ho KC (2014) Single layer of nickel hydroxide nanoparticles covered on a porous Ni foam and its application for highly sensitive non-enzymatic glucose, sensor. *Sens Actuators B* 204:159–166. <https://doi.org/10.1016/j.snb.2014.07.102>
- Chelaghmia ML, Nacef M, Affoune AM (2012) Ethanol electrooxidation on activated graphite supported platinum-nickel in

- alkaline medium. *J Appl Electrochem* 42:819–826. <https://doi.org/10.1007/s10800-012-0440-2>
28. Mao W, He H, Ye Z, Huang J (2019) Three-dimensional graphene foam integrated with Ni(OH)<sub>2</sub> nanosheets as a hierarchical structure for non-enzymatic glucose sensing. *J Electroanal Chem* 832:275–283. <https://doi.org/10.1016/j.jelechem.2018.11.016>
  29. Jia L, Wei X, Lv L, Zhang X, Duan X, Xu Y, Liu K, Wang J (2018) Electrodeposition of hydroxyapatite on nickel foam and further modification with conductive polyaniline for non-enzymatic glucose sensing. *Electrochim Acta* 280:315–322. <https://doi.org/10.1016/j.electacta.2018.05.130>
  30. Zhang Y, Zhao D, Zhu W, Zhang W, Yue Z, Wang J, Wang R, Zhang D, Wang J, Zhang G (2018) Engineering multistage nickel oxide rod-on-sheet nanoarrays on Ni foam: A superior catalytic electrode for ultrahigh-performance electrochemical sensing of glucose. *Sens Actuators B Chem* 255:416–423. <https://doi.org/10.1016/j.snb.2017.08.078>
  31. Ramkumar KD, Abraham WS, Viyash V, Arivazhagan N, Rabel AM (2017) Investigations on the microstructure, tensile strength and high temperature corrosion behaviour of Inconel 625 and Inconel 718 dissimilar joints. *J Manuf Process* 25:306–322. <https://doi.org/10.1016/j.jmapro.2016.12.018>
  32. Shakil M, Ahmad M, Tariq NH, Hasan BA, Akhter JI, Ahmed E, Mehmood M, Choudhry MA, Iqbal M (2014) Microstructure and hardness studies of electron beam welded Inconel 625 and stainless steel 304L. *Vacuum* 110:121–126. <https://doi.org/10.1016/j.vacuum.2014.08.016>
  33. Carroll EB, Otis AR, Borgonia JP, Suh JO, Dillon PR, Shapiro AA, Hofmann DC, Liu ZK, Beese AM (2016) Functionally graded material of 304L stainless steel and inconel 625 fabricated by directed energy deposition: characterization and thermodynamic modeling. *Acta Mater* 108:46–54. <https://doi.org/10.1016/j.actamat.2016.02.019>
  34. Babu MS, Kiruba M, Dharuman N, Sundaravignesh S, Sankarapandian S, Prabu V, Berchmans LJ, Sreedhar G (2019) High-temperature oxidation and hot corrosion behavior of Er<sub>2</sub>Sn<sub>2</sub>O<sub>7</sub>+Inconel 625 composite. *Ceram Int* 45:17620–17629. <https://doi.org/10.1016/j.ceramint.2019.05.327>
  35. Urso M, Torrisi G, Boninelli S, Bongiorno C, Priolo F, Mirabella S (2019) Ni(OH)<sub>2</sub>@Ni core-shell nanochains as low-cost high-rate performance electrode for energy storage applications. *Sci Rep* 9:7736. <https://doi.org/10.1038/s41598-019-44285-1>
  36. Wu MS, Sie YJ, Yang SB (2019) Hollow mesoporous nickel dendrites grown on porous nickel foam for electrochemical oxidation of urea. *Electrochim Acta* 304:131–137. <https://doi.org/10.1016/j.electacta.2019.02.100>
  37. Nacef M, Chelaghmia ML, Khelifi O, Pontié M, Djelaibia M, Guerfa R, Bertagna V, Vautrin-UI C, Aisset F, Affoune AM (2021) Electrodeposited Ni on pencil graphite electrode for glycerol electrooxidation in alkaline media. *Int J Hydrog Energy* 46:37670–37678. <https://doi.org/10.1016/j.ijhydene.2020.07.104>
  38. Veerasubramani GK, Krishnamoorthy K, Kim SJ (2016) Improved electrochemical performances of binder-free CoMoO<sub>4</sub> nanoplate arrays@Ni foam electrode using redox additive electrolyte. *J Power Sources* 306:378–386. <https://doi.org/10.1016/j.jpowsour.2015.12.034>
  39. Ferrari AGM, Foster CW, Kelly PJ, Brownson DAC, Banks CE (2018) Determination of the electrochemical area of screen-printed electrochemical sensing platforms. *Biosensors* 8:53. <https://doi.org/10.3390/bios8020053>
  40. Jafarian M, Forouzandeh F, Danaee I, Gopal F, Mahjani MG (2009) Electrocatalytic oxidation of glucose on Ni and NiCu alloy modified glassy carbon electrode. *J Solid State Electrochem* 13:1171–1179. <https://doi.org/10.1007/s10008-008-0632-1>
  41. Mathew M, Sandhyarani N (2013) A highly sensitive electrochemical glucose sensor structuring with nickel hydroxide and enzyme glucose oxidase. *Electrochim Acta* 108:274–280. <https://doi.org/10.1016/j.electacta.2013.07.010>
  42. Laviron E (1979) General expression of the linear potential sweep voltammogram in the case of diffusionless electrochemical systems. *J Electroanal Chem* 101:19–28. [https://doi.org/10.1016/S0022-0728\(79\)80075-3](https://doi.org/10.1016/S0022-0728(79)80075-3)
  43. Mao H, Cao Z, Guo X, Liu M, Sun D, Sun Z, Ge H, Zhang Y, Song XM (2019) Enhanced electrocatalytic performance for the oxidation of methanol by hierarchical NiS/Ni(OH)<sub>2</sub>@polypyrrole/graphene oxide nanosheets. *Appl Surf Sci* 471:355–367. <https://doi.org/10.1016/j.apsusc.2018.11.188>
  44. Chelaghmia ML, Fisli H, Nacef M, Brownson DAC, Affoune AM, Satha H, Banks CE (2021) Disposable non-enzymatic electrochemical glucose sensors based upon screen-printed graphite macroelectrodes modified via a facile methodology with Ni, Cu, and Ni/Cu hydroxides are shown to accurately determine glucose in real human serum blood samples. *Anal Methods* 13:2812–2822. <https://doi.org/10.1039/D1AY00056J>
  45. Dong M, Hu H, Ding S, Wang C (2021) High-performance non-enzymatic glucose-sensing electrode fabricated by a-nickel hydroxide-reduced graphene oxide nanocomposite on nickel foam substrate. *J Mater Sci Mater Electron* 32:19327–19338. <https://doi.org/10.1007/s10854-021-06451-y>
  46. Wang L, Xie Y, Wei C, Lu X, Li X, Song Y (2015) Hierarchical NiO superstructures/foam Ni electrode derived from Ni metal-organic framework flakes on foam Ni for glucose sensing. *Electrochim Acta* 174:846–852. <https://doi.org/10.1016/j.electacta.2015.06.086>
  47. Zhaoa Y, Gub G, Youa S, Jic R, Suota H, Zhaota C, Liu F (2015) Preparation of Ni(OH)<sub>2</sub> nanosheets on Ni foam via direct precipitation method for highly sensitive non-enzymatic glucose sensor. *RSC Adv* 5:53665–53670. <https://doi.org/10.1039/C5RA06664F>
  48. Xiao Q, Wang X, Huang S (2017) Facile synthesis of Ni(OH)<sub>2</sub> nanowires on nickel foam via one step low-temperature hydrothermal route for non-enzymatic glucose sensor. *Mater Lett* 198:19–22. <https://doi.org/10.1016/j.matlet.2017.03.172>
  49. Joa HJ, Shita A, Jhonc HS, Park SY (2020) Highly sensitive non-enzymatic wireless glucose sensor based on Ni–Co oxide nanoneedle-anchored polymer dots. *J Ind Eng Chem* 89:485–493. <https://doi.org/10.1016/j.jiec.2020.06.028>
  50. Lu W, Qin X, Asiri AM, Al-Youbi AO, Sun X (2013) Ni foam: a novel three-dimensional porous sensing platform for sensitive and selective nonenzymatic glucose detection. *Analyst* 138:417–420. <https://doi.org/10.1039/C2AN36138H>
  51. Huo H, Zhao Y, Xu C (2014) 3D Ni<sub>3</sub>S<sub>2</sub> nanosheet arrays supported on Ni foam for high-performance supercapacitor and nonenzymatic glucose detection. *J Mater Chem A* 2:15111–15117. <https://doi.org/10.1039/C4TA02857K>
  52. Kumar S, Fu YP (2021) PANI/g-C<sub>3</sub>N<sub>4</sub> composite over ZnCo<sub>2</sub>O<sub>4</sub>/Ni-foam, a bi-functional electrode as a supercapacitor and electrochemical glucose sensor. *Sustain Energy Fuels* 5:3987–4001. <https://doi.org/10.1039/D1SE00491C>
  53. Iwu KO, Lombardo A, Sanz R, Scire S, Mirabella S (2016) Facile synthesis of Ni nanofoam for flexible and low-cost non-enzymatic glucose sensing. *Sens Actuators B: Chem* 224:764–771. <https://doi.org/10.1016/j.snb.2015.10.109>
  54. Wang X, Wang M, Feng S, He D, Jiang P (2020) Controlled synthesis of flower-like cobalt phosphate microsheet arrays supported on Ni foam as a highly efficient 3D integrated anode for non-enzymatic glucose sensing. *Inorg Chem Front* 7:108–116. <https://doi.org/10.1039/C9QI00948E>
  55. Xia K, Yang C, Chenb Y, Tianb L, Sub Y, Wang J, Li L (2017) In situ fabrication of Ni(OH)<sub>2</sub> flakes on Ni foam through

- electrochemical corrosion as high sensitive and stable binder-free electrode for glucose sensing. *Sens Actuators B* 240:979–987. <https://doi.org/10.1016/j.snb.2016.09.077>
56. Guo Q, Zeng W, Li Y (2019) Highly sensitive non-enzymatic glucose sensor based on porous NiCo<sub>2</sub>O<sub>4</sub> nanowires grown on nickel foam. *Mater Lett* 256:126603. <https://doi.org/10.1016/j.matlet.2019.126603>
57. Chandrasekaran NI, Matheswaran M (2019) A sensitive and selective non-enzymatic glucose sensor with hollow Ni-AlMn layered triple hydroxide nanocomposites modified Ni foam. *Sens Actuators B: Chem* 288:188–194. <https://doi.org/10.1016/j.snb.2019.02.102>

**Publisher's Note** Springer Nature remains neutral with regard to jurisdictional claims in published maps and institutional affiliations.

Springer Nature or its licensor (e.g. a society or other partner) holds exclusive rights to this article under a publishing agreement with the author(s) or other rightsholder(s); author self-archiving of the accepted manuscript version of this article is solely governed by the terms of such publishing agreement and applicable law.